Computers and Structures 161 (2015) 31–42

Contents lists available at ScienceDirect

Computers and Structures

journal homepage: www.elsevier.com/locate/compstruc

Modeling strongly non-Gaussian non-stationary stochastic processes using the Iterative Translation Approximation Method and Karhunen–Loève expansion

Hwanpyo Kim, Michael D. Shields *

Department of Civil Engineering, Johns Hopkins University, MD, USA

ARTICLE INFO

Article history:
Received 21 March 2015
Accepted 12 August 2015

Keywords:
Non-Gaussian stochastic process
Non-stationary stochastic process
Iterative Translation Approximation Method
Karhunen–Loève expansion
Translation process theory
Evolutionary spectrum

ABSTRACT

A method is proposed for modeling non-Gaussian and non-stationary random processes using the Karhunen–Loève expansion and translation process theory that builds upon an existing family of procedures called the Iterative Translation Approximation Method (ITAM). The new method improves the ITAM by iterating directly on the non-stationary autocorrelation function. The existing ITAM requires estimation of the evolutionary spectrum from the autocorrelation function for which no unique relation exists. Consequently, computationally expensive estimates or simplifying assumptions/approximations reduced the ITAM performance for non-stationary processes. The proposed method improves the accuracy of the resulting process while maintaining computational efficiency. Several examples are provided.

1. Introduction

Problems having strong nonlinearities and significant uncertainty merge in diverse engineering fields – particularly in mechanics. With increasing computational power and developments in parallel computing, Monte Carlo simulation (MCS) has become an increasingly tractable method for solving stochastic engineering problems. For problems where the stochasticity is represented by random processes or fields, MCS requires the generation of sample realizations of the stochastic process/field. Methods for simulating Gaussian random processes are well developed – owing to the fact that they can be completely described by their first two moments. However, most real stochastic processes do not follow the Gaussian distribution. Simulation of non-Gaussian processes is a significantly more challenging and practically important problem, but its progress has been slow given the complexity of non-Gaussian stochastic processes. The problem is even further complicated when the process is also non-stationary.

The problem of simulating non-Gaussian stochastic processes has attracted significant interest in the past twenty years. This research has spawned the development of methods rooted in two different basic simulation algorithms: the spectral representation method (SRM) and Karhunen–Loève (K–L) expansion. The K–L expansion [1,2] was originally utilized for simulating stationary and non-stationary Gaussian stochastic processes. Phoon et al. [3,4] proposed a method to simulate samples of non-stationary and non-Gaussian processes that makes use of the K–L expansion by iteratively updating the distribution of the underlying non-Gaussian K–L random variables. Around the same time, Sakamoto and Ghanem [5,6] proposed a method that utilizes a Polynomial Chaos expansion of K–L random variables to produce realizations of non-stationary and non-Gaussian stochastic processes. Another class of algorithms is based on the SRM, which was also initially utilized for simulating stationary and non-stationary Gaussian stochastic processes [7,8]. Combining the SRM with translation process theory [9] enables the simulation of stochastic processes according to a prescribed power spectral density function (PSDF) (equivalently, autocorrelation function (ACF)) and marginal non-Gaussian cumulative distribution function (CDF). The challenge with these translation-based methods is to identify an underlying Gaussian PSDF that, when mapped using translation process theory, yields a non-Gaussian PSDF that matches the prescribed target. Several researchers have proposed methods to do so including Yamazaki and Shinozuka [10], Deodatis and Micaletti [11], and Bocchini and Deodatis [12]. Recently, Shields et al. [13–15] developed a class of conceptually simple and efficient iterative methods for simulation of non-Gaussian translation processes (collectively

* Corresponding author.
E-mail addresses: khwanpy1@jhu.edu (H. Kim), michael.shields@jhu.edu (M.D. Shields).

http://dx.doi.org/10.1016/j.compstruc.2015.08.010
0045-7949/

referred to as Iterative Translation Approximation Method – ITAM). However, for non-stationary processes, the ITAM requires estimation of the evolutionary spectrum (ES) as defined by Priestley [16] that can be quite challenging [15,17].

The present paper proposes an efficient methodology for simulating non-stationary and strongly non-Gaussian stochastic processes based on the ITAM that utilizes the K–L expansion. The methodology improves the accuracy and efficiency of the ITAM for these processes because it does not require approximation of the evolutionary spectrum. Instead, it upgrades directly the underlying Gaussian ACF. As with previous ITAM methodologies, it is conceptually simple, straightforward to implement, and converges very rapidly to an underlying Gaussian ACF that, when mapped to the non-Gaussian distribution, matches the target ACF with high accuracy. By definition, the resulting process also possesses the target non-Gaussian marginal distribution.

2. Karhunen–Loève expansion

Consider a general random process $A(x,\theta)$ defined on the probability space (Ω,σ,P) indexed on x over the domain D with mean $\bar{A}(x)$ and finite variance $E[(A(x,\theta)-\bar{A}(x))^2]$. The process can be expressed as:

$$A(x,\theta)=\bar{A}(x)+\sum_{i=1}^{\infty}\sqrt{\lambda_i}\zeta_i(\theta)f_i(x) \tag{1}$$

where λ_i and $f_i(x)$ are the eigenvalues and eigenvectors of the covariance function $C(x_1,x_2)$. The covariance function $C(x_1,x_2)$ has the following spectral decomposition:

$$C(x_1,x_2)=\sum_{i=1}^{\infty}\lambda_i f_i(x_1)f_i(x_2) \tag{2}$$

where its eigenvalues and eigenvectors are determined by solving the homogenous Fredholm integral equation of the second kind given by:

$$\int_D C(x_1,x_2)f_i(x_1)dx_1=\lambda_i f_i(x_2) \tag{3}$$

the solution of which must be determined numerically for problems of practical interest [1,18]. The eigenvectors form a complete orthogonal set of basis functions for the random process following the equation:

$$\int_D f_i(x)f_j(x)dx=\delta_{ij} \tag{4}$$

where δ_{ij} is the Kronecker-delta function and the parameters $\zeta_i(\theta)$ in Eq. (1) denote a set of uncorrelated random variables with zero mean and unit variance given by:

$$\zeta_i(\theta)=\frac{1}{\sqrt{\lambda_i}}\int_D\left[A(x,\theta)-\bar{A}(x)\right]f_i(x)dx \tag{5}$$

In practice, the series in Eq. (1) is approximated using a finite number, M, of eigenvalues and eigenvectors as:

$$\tilde{A}(x,\theta)=\bar{A}(x)+\sum_{i=1}^{M}\sqrt{\lambda_i}\zeta_i(\theta)f_i(x) \tag{6}$$

Eq. (6) is used for simulation purposes by generating the $\zeta_i(\theta)$.

For Gaussian processes, $\zeta_i(\theta)$ are Gaussian. But for non-Gaussian processes, they are generally non-Gaussian and, in order to determine their distributions, Eq. (5) must be solved. Moreover, they may exhibit higher-order dependencies/correlations that are difficult or impossible to identify [19]. The integrand in Eq. (5) is obviously unknown thus requiring iterative methods such as those proposed by Phoon et al. [3,4]. These have proven useful for many applications but it is important to point out that these methods are being counteracted by the Central Limit Theorem; thus limiting their ability to match strongly non-Gaussian distributions. In other words, the K–L expansion based simulation methods typically assume $\zeta_i(\theta)$ are independent and consequently these processes tend to Gaussian as $M\to\infty$ [19]. In fact, even for small M the processes will tend to be "more Gaussian" than is desirable given the present applications.

3. Translation process theory

An alternate means of constructing non-Gaussian stochastic processes utilizes Grigoriu's translation process theory [9] wherein a Gaussian process, $X(t)$, is mapped via a nonlinear transformation to a non-Gaussian process, $Y(t)$. In general, for stationary processes this is expressed as:

$$Y(t)=g(X(t)) \tag{7}$$

with $g(\cdot)=F_N^{-1}\{\Phi[\cdot]\}$ referred to as the standard translation that maps a process from the Gaussian distribution $\Phi(\cdot)$ to the non-Gaussian distribution with marginal CDF $F_N(\cdot)$. In this work, we are concerned with non-stationary processes for which Ferrante et al. [20] have extended translation process theory as discussed in the following.

Let $X(t)$ be a stationary and Gaussian stochastic process with zero mean and unit variance. The non-stationary and non-Gaussian process $Y(t)$ with (in general, time varying) marginal CDF $F_N(\cdot,t)$ is mapped from the stationary Gaussian process $X(t)$ through:

$$Y(t)=g(X(t),t)=F_N^{-1}\{\Phi[X(t)],t\} \tag{8}$$

where $F_N^{-1}(\cdot,t)$ is the inverse marginal non-Gaussian CDF at time t and $\Phi(\cdot)$ is the stationary and Gaussian CDF with zero mean and unit variance. The non-stationary and non-Gaussian ACF of $Y(t)$ can be determined by:

$$\begin{aligned}R_N(s,t)&=\mu(s)\mu(t)+\sigma(s)\sigma(t)\xi(s,t)\\&=\int_{-\infty}^{\infty}\int_{-\infty}^{\infty}g(x_1,s)g(x_2,t)\phi\{x_1,x_2;\rho(s,t)\}\,dx_1\,dx_2\end{aligned} \tag{9}$$

where $\mu(t)$ and $\sigma(t)$ are the mean and the standard deviation of $Y(t)$ at time t, $\xi(s,t)$ is its normalized ACF (also referred as the correlation distortion), and $\phi\{\cdot,\cdot;\rho(s,t)\}$ is the joint Gaussian probability density function (PDF) with normalized Gaussian ACF $\rho(s,t)$, given by:

$$\phi\{x_1,x_2;\rho(s,t)\}=\frac{1}{\sqrt{2\pi(1-\rho(s,t)^2)}}\exp\left(-\frac{x_1^2+x_2^2-2\rho(s,t)x_1x_2}{2(1-\rho(s,t)^2)}\right). \tag{10}$$

Eq. (9) can be solved using standard numerical quadrature rules. In our implementation, numerical integration was conducted using the quad2D function in Matlab and found to be sufficiently accurate. A description of the numerical algorithm can be found in [21]. The cost of this integration depends heavily on the form of $g(x,t)$ and is discussed more specifically in the provided examples. The forward translation in Eq. (9), that maps a known underlying Gaussian process to a prescribed non-Gaussian distribution, is always possible. However, the inverse transformation – the case of a given non-Gaussian ACF and an unknown Gaussian ACF – does not always have an exact solution. In such cases, the pair of ACF and non-Gaussian marginal distribution is said to be incompatible. Ferrante et al. [20] identified two specific cases in which non-stationary translation process incompatibility arises:

1. The inversion of Eq. (9) yields an underlying Gaussian correlation function that is not positive semi-definite (PSD). When the ACF is not PSD, it is not admissible as an ACF. For practical purposes, this is checked by computing the eigenvalues of the ACF $\rho(t,s)$. If it possesses negative eigenvalues then the ACF is not PSD.
2. The normalized non-Gaussian correlation $\xi(s,t)$ has certain values that lie outside of its admissible range $[\xi^{\min}(s,t), \xi^{\max}(s,t)]$. The acceptable bounds for the non-Gaussian correlation distortion are calculated by setting $\rho(s,t) = 1$ and -1 in Eq. (8) to obtain the upper and lower bounds respectively. In the non-stationary case, the bounds on the non-Gaussian correlation are time dependent with $\xi^{\min}(s,t) = -\xi^{\max}(s,t)$ if the non-Gaussian CDF is an odd function at either time s or t. Note also that the upper bound is not necessarily unity as in the stationary case.

4. Iterative Translation Approximation Method

There are many problems where the translation process model is useful despite the incompatibility. In particular, it is useful to identify a Gaussian process that, when translated, matches the prescribed target non-Gaussian ACF as closely as possible. This is particularly important for those problems that are sensitive to the distribution. This is true, for example, when the extreme values are critical to the analysis such as in reliability analysis or when the stochastic process is applied to a model with strong nonlinearities. Conversely, in cases where accurate correlations drive response (such as those where quantities of interest involve integrals over stochastic processes) an alternative approach that more accurately resolves correlations at the expense of the distribution may be more appropriate. In this work, we are specifically interested in the former case where accuracy in distribution is of paramount importance.

To manage the incompatible cases, Shields et al. [13] proposed a methodology, referred to as the ITAM, to simulate a non-Gaussian and stationary processes by iteratively upgrading the Gaussian PSDF using SRM. Shields and Deodatis [15] extended the ITAM for non-stationary and non-Gaussian processes by iteratively upgrading the underlying Gaussian ES. Given a target non-Gaussian and non-stationary ES, $S_N^T(\omega,t)$, the ITAM iteratively upgrades the underlying Gaussian ES as:

$$S_G^{(i+1)}(\omega,t) = \left[\frac{S_N^T(\omega,t)}{S_N^{(i)}(\omega,t)}\right]^{\beta} S_G^{(i)}(\omega,t) \tag{11}$$

where $S_N^{(i)}(\omega,t)$ is the estimated non-Gaussian ES at iteration i, $S_G^{(i)}(\omega,t)$ and $S_G^{(i+1)}(\omega,t)$ are the underlying Gaussian ES at iteration i and $i+1$ respectively, and the exponent β is selected to optimize convergence speed. The ITAM has several advantages: (1) It generally converges in ten iterations or less; (2) It is computationally inexpensive and straightforward to implement; (3) The underlying Gaussian ES satisfies all compatibility conditions imposed by translation process theory, and; (4) The computed non-Gaussian ES is very close to the target. The primary drawback of the ITAM for non-stationary processes is that it requires estimation of the ES from the non-stationary ACF. As defined by Priestley [16], the non-stationary ACF does not uniquely define an ES. Recently, Benowitz et al. [17] have explored this uniqueness and proposed a method to compute a unique ES from the non-stationary ACF under certain conditions. This method, however, is computationally very expensive. For the ITAM development, Shields and Deodatis [15] proposed an approximate quantity called the pseudo-autocorrelation that assumes local stationarity. Consequently, to apply the ITAM method for non-stationary and non-Gaussian processes requires either a tremendous computation burden or an additional layer of approximation. The extension of the ITAM proposed herein alleviates both of these potential pitfalls.

5. Proposed ITAM with Karhunen–Loève expansion

The proposed methodology bypasses the estimation of the ES by iteratively upgrading the underlying non-stationary ACF directly and simulating the process using the K–L expansion. The new method, denoted KL-ITAM, for estimating the underlying Gaussian ACF proceeds according to the following general steps:

(1) Initialize the underlying Gaussian ACF.
(2) Compute the non-Gaussian ACF from non-stationary translation process theory.
(3) Upgrade the underlying Gaussian ACF.
(4) Find the nearest positive semi-definite (PSD) ACF to the upgraded Gaussian ACF.
(5) Check the difference between the estimated and target ACFs and iterate back to step 2.
(6) Simulate the process using the K–L expansion.

The procedure is provided in the flowchart in Fig. 1 as well. The following sections explain the particulars of the proposed methodology.

5.1. Initialize underlying Gaussian ACF

Given a prescribed pair of marginal non-Gaussian CDF and non-stationary ACF, select an arbitrary underlying Gaussian ACF as an initial guess. The ACF must, obviously, satisfy all conditions of a valid ACF. Practically, this can be achieved by selecting the target non-Gaussian ACF as the initial underlying Gaussian ACF.

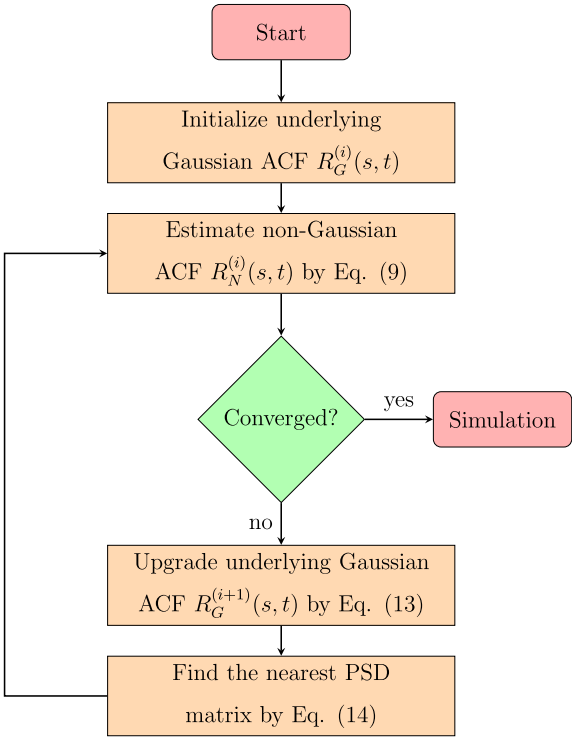

Fig. 1. Flowchart of proposed KL-ITAM methodology.

5.2. Compute the non-Gaussian ACF

Next, calculate the non-Gaussian and non-stationary ACF from the prescribed underlying Gaussian and non-stationary ACF using translation process theory. To accomplish this, the normalized Gaussian correlation function is computed as:

$$\rho^{(i)}(s,t) = \frac{R_G^{(i)}(s,t)}{\sqrt{R_G^{(i)}(t,t)\cdot R_G^{(i)}(s,s)}} \tag{12}$$

where $R_G^{(i)}(t,t)$ is the variance of the underlying Gaussian process at time t. The normalized Gaussian ACF is translated to the non-Gaussian ACF $R_N(s,t)$ using Eq. (9).

5.3. Upgrade underlying Gaussian ACF

If the procedure is not converged at iteration i, upgrade the underlying Gaussian ACF for iteration $i+1$ using the following equation:

$$R_G^{(i+1)}(s,t) = \left(\frac{R_N^T(s,t)}{R_N^{(i)}(s,t)}\right) R_G^{(i)}(s,t) \tag{13}$$

The proposed equation is based on the upgrading equation in [15] (Eq. (11)). However, the upgraded ACF is not strictly non-negative in contrast with the ES in the standard ITAM. For this reason, the exponent β is eliminated as any non-integer exponent will produce imaginary numbers when the signs of $R_G^{(i)}(s,t)$ and $R_N^T(s,t)$ differ. Furthermore, the new upgrading equation does not guarantee the upgraded ACF is PSD. Consequently, an additional step for maintaining the PSD property of the ACF at each iteration is necessary.

5.4. Find nearest positive semi-definite ACF

Given an arbitrary real, symmetric matrix A, Higham [22] proposed a method for calculating its nearest correlation matrix in Frobenius norm by solving:

$$\begin{aligned} &\min \ \|A-\hat{A}\|_F \\ &\text{s.t.} \quad \hat{A}=\hat{A}^T, \quad \mathrm{Diag}(\hat{A})=e, \quad \hat{A}\geq 0 \end{aligned} \tag{14}$$

where e is the unit vector, $\hat{A}$ is the nearest PSD matrix, and $\mathrm{Diag}(\hat{A})$ denotes a vector of the diagonal elements of $\hat{A}$. The method utilizes convex analysis to identify the solution and it is shown to converge linearly to the solution. Subsequently, Qi and Sun [23] presented a quadratically convergent Newton method for finding the nearest correlation matrix by dualizing Eq. (14) to an unconstrained convex optimization problem. Although various methodologies exist for computing the nearest PSD matrix including the method of Borsdorf and Higham [24], the paper only focuses on the prescribed scheme of Qi and Sun. Our implementation utilizes this algorithm; details of which can be found in Appendix A. Given the quadratic convergence of the algorithm in [23], the optimization converges rapidly to the nearest PSD matrix, but is dependent upon the degree of incompatibility between the target non-Gaussian ACF and the prescribed distribution. For nearly compatible or compatible cases, the optimization is not necessary, while, for highly incompatible cases the optimizer may require up to five iterations of the Newton-conjugate gradient (CG) method. These iterations are computationally inexpensive (generally conducted in a fraction of a second in Matlab on a single 2.3 GHz Intel Core i7 processor).

The step of finding the nearest PSD correlation matrix is implemented after upgrading the underlying Gaussian ACF at each iteration. Even though the computed non-Gaussian and non-stationary ACF is closer to the target without this step, the converged underlying ACF is not PSD (and, therefore, not a valid ACF). In this case, the underlying Gaussian ACF has negative eigenvalues and simulation with the K–L expansion produces considerable numerical errors. This is explored further in Section 8.

5.5. Check relative difference and iterate

At each iteration, the relative difference between the target non-Gaussian non-stationary ACF and the computed one is determined by:

$$\epsilon_{(i)} = 100\sqrt{\frac{\sum_{n=0}^{N-1}\sum_{m=0}^{N-1}\left[R_N^{(i)}(s_n,t_m)-R_N^T(s_n,t_m)\right]^2}{\sum_{n=0}^{N-1}\sum_{m=0}^{N-1}\left[R_N^T(s_n,t_m)\right]^2}} \tag{15}$$

where N is the number of time intervals in the discretized domain. According to the value of the relative difference, the iterative procedure will continue or stop. Specifically, when the difference stabilizes to a constant value, the iterations are stopped.

5.6. Simulation using K–L Expansion

The iterative process produces an underlying Gaussian ACF that, when translated to the target non-Gaussian distribution, matches the target non-Gaussian and non-stationary ACF very closely. After obtaining the converged underlying Gaussian ACF, simulation of the Gaussian process proceeds by the K–L expansion given in Eq. (6). The generated Gaussian and non-stationary sample functions are mapped to the non-Gaussian and non-stationary form using Eq. (8). Thus, the K–L expansion can be employed with Gaussian random variables to generate the underlying Gaussian process unlike in the previous methods that require identifying the distribution of the non-Gaussian K–L random variables.

5.7. Comments on numerical implementation

From a numerical perspective, there are very few limitations beyond the typical issues associated with discretization/truncation of the K–L expansion as studied by Huang et al. [2]. In our implementation, all eigenvalues and eigenvectors from the numerical K–L expansion are kept. Thus, numerical issues arise only in the selection of the appropriate discretization of the ACF. Furthermore, given the right discretization of the ACF, it is possible to consider processes of any length. The accuracy of the proposed ITAM approach is very high regardless of the discretization. In other words, however the user discretizes the ACF, the method will match it very accurately. Of course, the discretization of the ACF should be conducted in accordance with standard practices [2] given the user's desired accuracy and computational constraints. In general, as the discretization becomes finer the ACF representation improves but the numerical ACF matrix grows in size exponentially. This effects the cost of the upgrading because it requires an exponentially growth in the number of evaluation of Eq. (9). This expense can be offset to a large degree by pre-computing Eq. (9) at discrete intervals and interpolating as suggested in [13].

6. Numerical examples

To verify the efficiency of the proposed methodology, several numerical examples of both stationary and non-stationary and strongly and weakly non-Gaussian processes are considered. Additionally, examples are considered that explicate both types of the translation process incompatibility described in Section 3. The

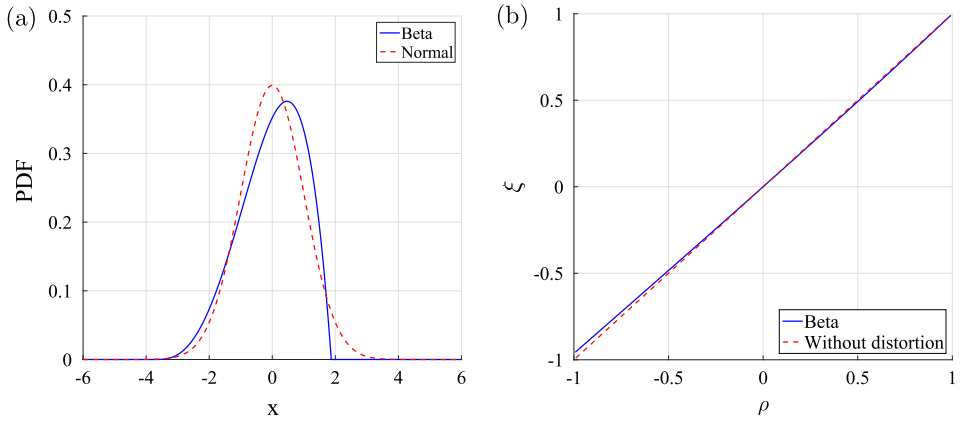

Fig. 2. (a) Weakly non-Gaussian and stationary beta pdf and (b) its correlation distortion.

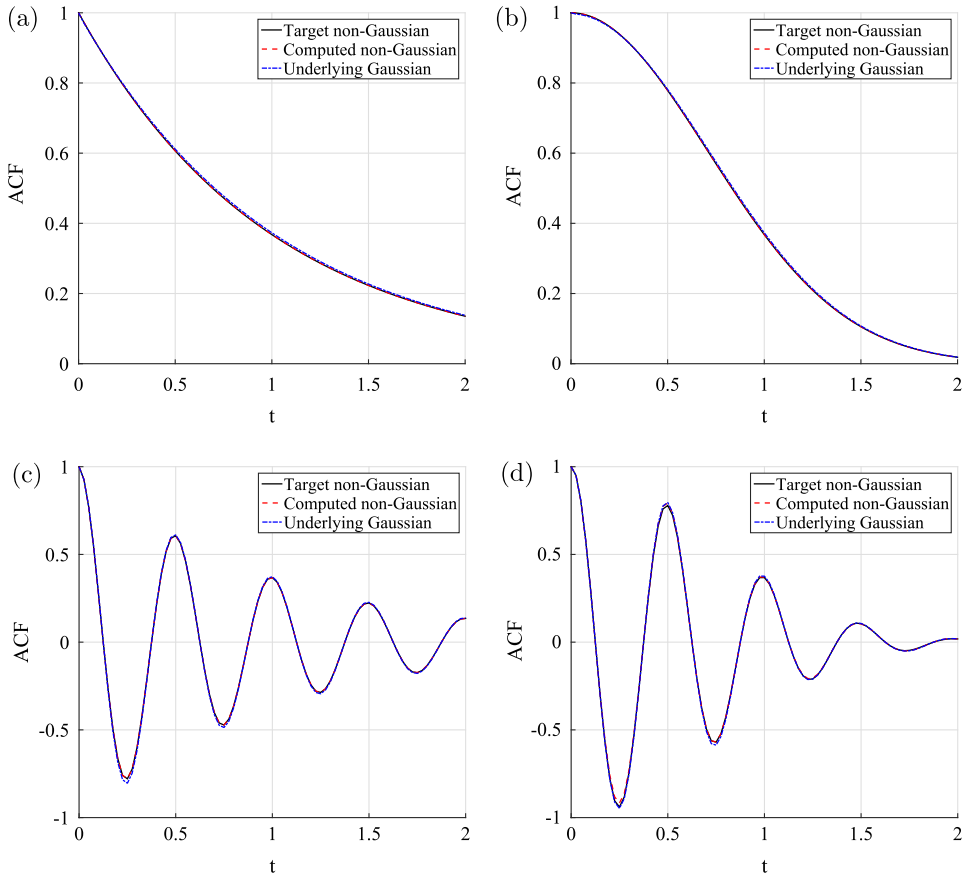

Fig. 3. Underlying Gaussian, target non-Gaussian and KL-ITAM computed non-Gaussian ACFs for (a) C_1, (b) C_2, (c) C_3, and (d) C_4 with weakly non-Gaussian beta distribution.

same and modified numerical examples in Phoon et al. [3] are utilized.

6.1. Stationary and non-Gaussian processes

The following target non-Gaussian and stationary ACFs are investigated:

$$\begin{aligned} C_1(s,t) &= \exp(-|s-t|) \\ C_2(s,t) &= \exp(-|s-t|^2) \\ C_3(s,t) &= \exp(-|s-t|)\cdot\cos[4\pi(s-t)] \\ C_4(s,t) &= \exp(-|s-t|^2)\cdot\cos[4\pi(s-t)] \end{aligned} \tag{16}$$

where all processes are defined over the interval $s,t\in[0,2]$.

Two different zero mean and unit standard deviation marginal non-Gaussian CDFs are selected to explore the accuracy and efficiency of the presented methodology for weakly and strongly non-Gaussian processes.

The beta distribution has CDF given by:

$$F(y;p,q)=\frac{\Gamma(p+q)}{\Gamma(p)\Gamma(q)}\int_0^u z^{p-1}(1-z)^{q-1}dz \tag{17}$$

where $u=\frac{y-y_{\min}}{y_{\max}-y_{\min}}$ with upper and lower bounds $y_{\min}$ and $y_{\max}$, and $\Gamma(\cdot)$ is the gamma function. The distribution parameters are selected to be $p=4$ and $q=2$ to produce zero mean and unit

Table 1
Relative differences and computational costs for KL-ITAM given weakly (beta) and strongly (lognormal) non-Gaussian distributions applied to stationary and non-stationary processes.

Target	Beta distribution			
	Relative diff., ϵ (%)	KL-ITAM iter.	CPU time (s)	Max. Newton-CG iter.
Stationary ($\Delta x = 0.0250$, 81×81 matrices)				
C_1	0.0000	3	667	0
C_2	0.0599	4	765	1
C_3	0.0000	3	562	0
C_4	1.9372	3	573	3
Non-stationary ($\Delta x = 0.0125$, 81×81 matrices)				
C_5	0.0024	7	1773	0
C_6	0.0007	6	1156	0
C_7	0.0007	6	1165	0
C_8	0.0009	6	1016	0
Target	Lognormal distribution			
	Relative diff., ϵ (%)	KL-ITAM iter.	CPU time (s)	Max. Newton-CG iter.
Stationary ($\Delta x = 0.0250$, 81×81 matrices)				
C_1	0.0416	10	964	0
C_2	0.2277	11	1037	4
C_3	35.393	5	374	5
C_4	39.925	4	316	5
Non-stationary ($\Delta x = 0.0125$, 81×81 matrices)				
C_5	0.0159	14	1584	0
C_6	0.0142	10	851	0
C_7	34.450	4	341	5
C_8	22.685	5	379	4

variance, and the upper and lower bound of the distribution are $y_{\min} = -3.74$ and $y_{\max} = 1.87$. According to plots of the PDF and the correlation distortion in Fig. 2, the target beta distribution is considered weakly non-Gaussian and the correlation distortion of this beta distribution is small.

The non-Gaussian and stationary ACFs (C_1–C_4) resulting from KL-ITAM iterations with the beta distribution are shown with their respective target ACFs and the corresponding underlying Gaussian ACFs in Fig. 3. The change of distribution from Gaussian to beta distorts the ACFs only slightly, and the incompatibility does not appear significantly. To evaluate the efficacy of the presented methodology, the relative difference between the target and ITAM computed non-Gaussian ACFs from Eq. (15) are given in Table 1. The maximum value of those differences is only 1.94%; thus the KL-ITAM calculated non-Gaussian ACFs are very close to their respective targets.

The shifted lognormal distribution has CDF given by:

$$F(y;\alpha,\beta,\delta) = \Phi\left(\frac{\ln(y-\delta)-\alpha}{\beta}\right) \tag{18}$$

To yield zero mean and unit variance, the distribution parameters are selected to be $\alpha = -0.7707, \beta = 1$, and $\delta = -0.7628$. This distribution is considered strongly non-Gaussian as demonstrated by Fig. 4, which plots the PDF and the correlation distortion. The correlation distortion, in this case, is very strong and possesses a large range of unacceptable values corresponding to large negative correlation.

The ACFs (C_1–C_4) for the strongly non-Gaussian process are shown in Fig. 5, which shows the underlying Gaussian, target non-Gaussian, and KL-ITAM computed non-Gaussian ACFs. Compared with the prescribed beta distribution, the distortion of the translation process is considerable. Despite the strongly non-Gaussian property of the prescribed distribution, the ITAM results are extremely accurate and efficient for ACFs C_1 and C_2 with relative differences of only 0.014% and 0.228%, respectively. This is because C_1 and C_2 posses only positive correlation where the distortion is small compared to the negative distortion and incompatibility of the second kind (Section 3) is not present. However, the prescribed ACFs C_3 and C_4 have much larger errors of 35.30% and

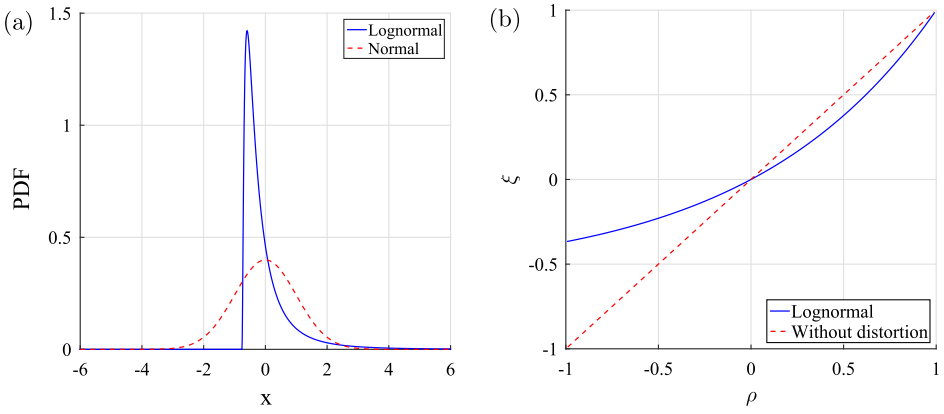

Fig. 4. (a) Strongly non-Gaussian and stationary shifted lognormal pdf and (b) its correlation distortion.

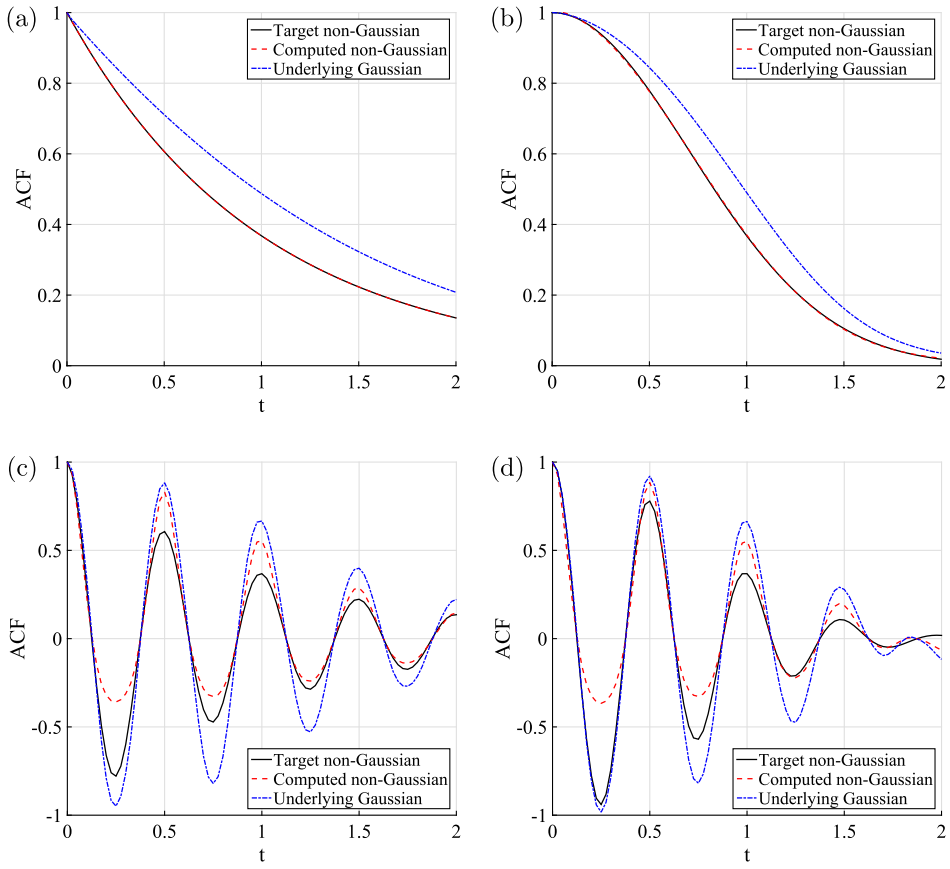

Fig. 5. Underlying Gaussian, target non-Gaussian, and ITAM computed non-Gaussian ACFs for (a) C_1, (b) C_2, (c) C_3, and (d) C_4 with strongly non-Gaussian shifted lognormal distribution.

39.92% respectively because of translation incompatibility in the range of negative correlation. Although the differences between the target and computed non-Gaussian ACFs with the strong distortion are large, the dominant characteristics of the target non-Gaussian and stationary ACFs are maintained in the computed ACFs. The differences lie purely in their magnitudes.

Summary results of the K–L ITAM method for C_1–C_4 are provided in Table 1 which presents the final relative error and the required number of iterations along with the associated computational cost. Note that the computational expense is due primarily to the numerical solution of Eq. (9) which needs to be solved several thousands times per iteration. The CPU times presented in Table 1 could be drastically reduced through parallelization (all computations are solved serially on a single 2.3 GHz Intel Core i7 processor), implementation in a lower level language (current implementation is in Matlab), and precomputation of the translation at selected values (i.e. generating a lookup table and interpolating). Also shown in Table 1, are the maximum number of the Newton-CG iterations across all K–L ITAM iterations.

6.2. Non-stationary and non-Gaussian processes

In this section, the following target non-stationary covariance functions are considered:

$$\begin{aligned} C_5(s,t) &= \min(s,t) \\ C_6(s,t) &= 4[\min(s,t) - st] \\ C_7(s,t) &= \min(s,t)\cos[4\pi(s-t)] \\ C_8(s,t) &= 4[\min(s,t) - st]\cos[4\pi(s-t)] \end{aligned} \tag{19}$$

The prescribed covariances are defined in the time domain $s,t \in [0,1]$ and the maximum variance is unity, for all. Plots of these target covariances are provided in Fig. 6, which shows that target covariance has time-dependent variance.

Two different non-Gaussian and non-stationary CDFs are again considered possessing zero mean and time-dependent variance corresponding to the target covariance functions.

The non-stationary beta distribution is considered with CDF given by Eq. (17) where $u = \frac{y-y_{\min}}{y_{\max}-y_{\min}}$, $y_{\min} = \mu_b(t) - \sigma_b(t)\sqrt{\frac{p(p+q+1)}{q}}$, and $y_{\max} = \mu_b(t) + \sigma_b(t)\sqrt{\frac{q(p+q+1)}{p}}$. The distribution parameters are selected to be $p = 4$ and $q = 2$, the mean $\mu_b(t) = 0$ and the variance $\sigma_b(t)^2 = C(t,t)\forall t$. A plot of the beta PDF with unit variance is shown in Fig. 2a. For the non-stationary beta distribution, the results of the proposed KL-ITAM methodology at time $t = 0.5$ are shown in Fig. 7. The relative differences are very close to zero in the converged states as summarized in Table 1. There is clearly very good agreement between the KL-ITAM computed and target non-Gaussian covariance and the underlying Gaussian can then be used for simulation purposes.

The non-stationary shifted lognormal distribution is considered with CDF given in Eq. (18). The shape of the marginal CDF is defined by the distribution parameter α and β where β is unity for all time. The parameters α and δ are functions of time and are determined by setting the mean $\mu_l(t) = 0$ and the variance $\sigma_l^2(t)$ equal to the target variance at time t. Thus, the mean and variance of the distribution are given by:

$$\mu_l(t) = \delta(t) + \exp\left[\alpha(t) + \frac{\beta^2}{2}\right] \tag{20}$$

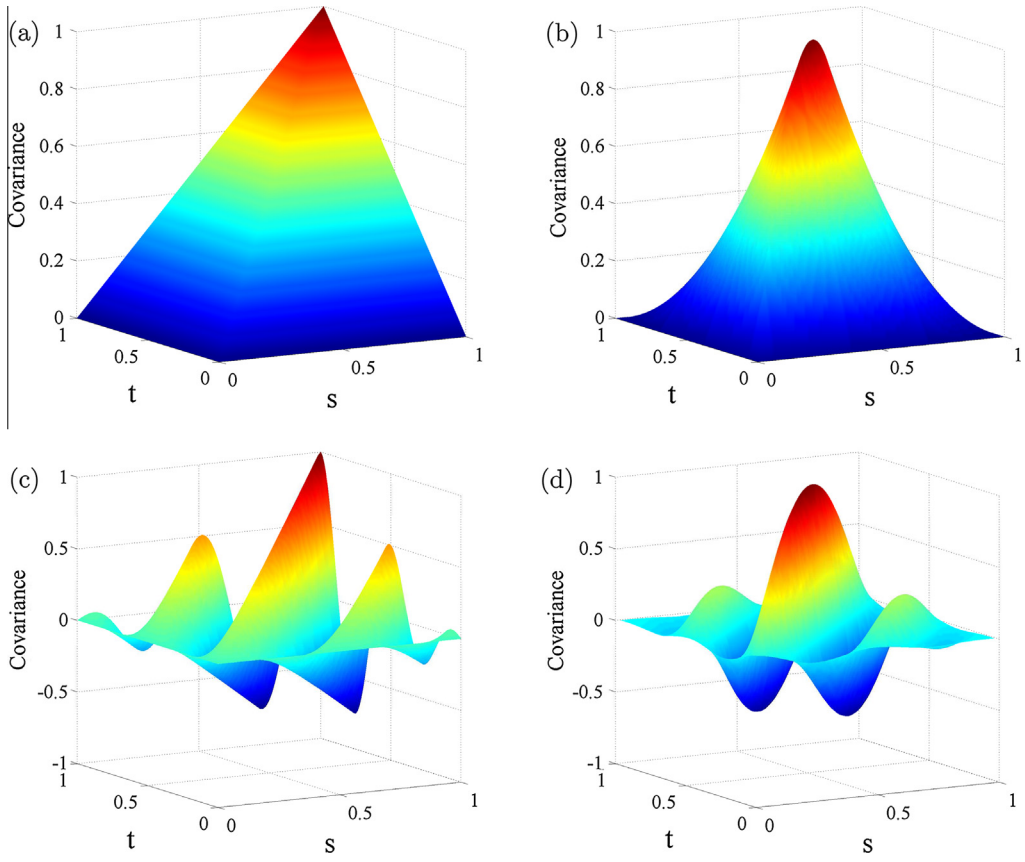

Fig. 6. Target non-stationary covariances: (a) C_5, (b) C_6, (c) C_7, and (d) C_8.

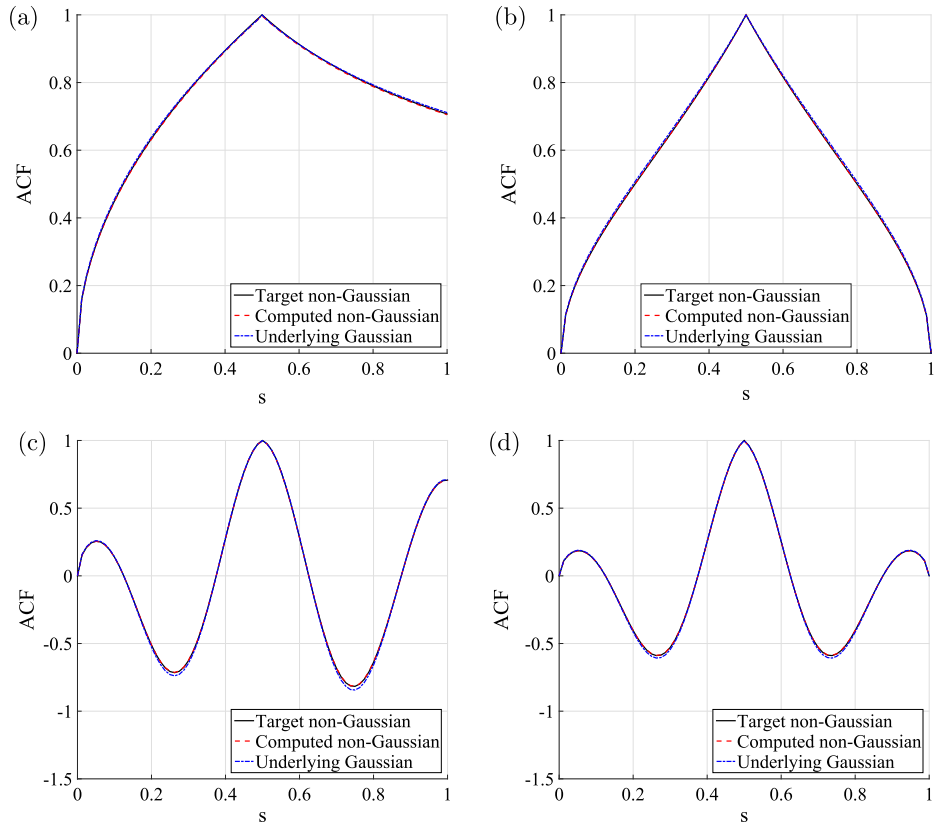

Fig. 7. Underlying Gaussian, target non-Gaussian, and KL-ITAM computed non-Gaussian normalized ACFs of (a) C_5, (b) C_6, (c) C_7, and (d) C_8 with non-stationary beta distribution at time $t = 0.5$.

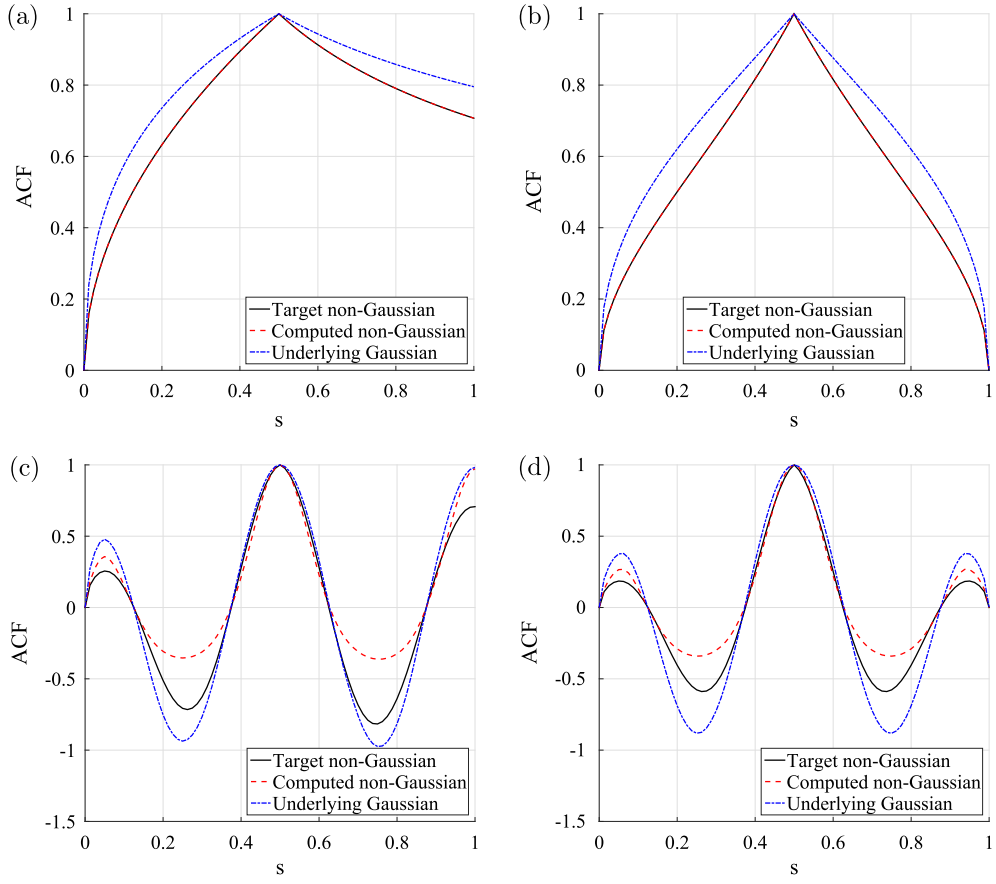

Fig. 8. Underlying Gaussian, target non-Gaussian, and KL-ITAM computed non-Gaussian normalized ACFs of (a) C_5, (b) C_6, (c) C_7, and (d) C_8 with non-stationary shifted lognormal distribution at time $t = 0.5$.

$$\sigma_l^2(t) = [\exp(\beta^2) - 1] \cdot \exp[2\alpha(t) + \beta^2] \tag{21}$$

A plot of the lognormal PDF with unit variance is shown in Fig. 4a. Results of the computed and underlying Gaussian normalized ACFs are plotted in Fig. 8 at time $t = 0.5$ and are summarized in Table 1. In the case of C_5 and C_6, the proposed methodology achieves a very high level of accuracy with relative differences between the target and computed non-Gaussian and non-stationary ACFs of only 0.016% and 0.014% respectively. However, the relative differences in the covariances C_7 and C_8 are much larger at 34.45% and 22.69% respectively. Similar to the stationary case, severe incompatibility of the ACF and CDF in the negative correlations prevents the computed normalized ACFs from converging to the target.

7. Comparison with the SRM-based ITAM

A primary benefit of the proposed method, when compared to the original SRM-based ITAM method for non-stationary and non-Gaussian processes is that it alleviates the burden and the additional level of approximation necessary in estimation of the ES. Hence, the proposed method improves the accuracy of the translation process. For direct comparison with the SRM-based ITAM by Shields and Deodatis [15], an example with strongly incompatible marginal PDF and non-Gaussian ES from that work is considered. The non-Gaussian ES is defined as:

$$S_N(\omega, t) = e^{-\left(\frac{\omega - \omega_0(t)}{2}\right)^2} \tag{22}$$

where the parameter $\omega_0(t)$ is defined as:

$$\omega_0(t) = 10 + 20t \tag{23}$$

The non-Gaussian and non-stationary ACF, which is equivalent to the non-Gaussian ES, is calculated using Priestley's theory of evolutionary power [16] as:

$$R_N(s,t) = \int_{-\infty}^{\infty} \sqrt{S_N(\omega, s) S_N(\omega, t)} e^{i\omega t} d\omega \tag{24}$$

The non-stationary and non-Gaussian ES and ACF are depicted in Fig. 9.

Two different beta distribution are considered with zero mean, unit standard deviation and PDF given by:

$$f(y; a, b, c, d) = \frac{\Gamma(c+d)}{\Gamma(c)\Gamma(d)(b-a)^{c+d-1}} (y-a)^{c-1} (b-y)^{d-1} \tag{25}$$

The first distribution is a "U-shaped" beta with parameters $a = -1.1$, $b = 1.7$, $c = 0.342$, and $d = 0.528$. The second is a "L-shaped" beta distribution with parameters $a = -0.457$, $b = 28.45$, $c = 0.1895$, and $d = 11.795$. The corresponding PDFs and correlation distortions are presented in Fig. 10. The bounds on the distributions are defined as $y_{\min} = a$, and $y_{\max} = b$. As noted in [15], both marginal probability distributions have significant incompatibility with the prescribed non-Gaussian ES/ACF.

The estimated compatible ACFs for the two beta distributions are calculated using the KL-ITAM and the relative differences at time instants $t = 0$, $t = 1$, and $t = 2$ are compared with the corresponding values obtained using the SRM-based ITAM in Table 2. Additionally, plots showing the converged ACF using KL-ITAM and SRM-ITAM compared to the target ACF for the two distributions are shown at different time instant in Fig. 11. It is clear that

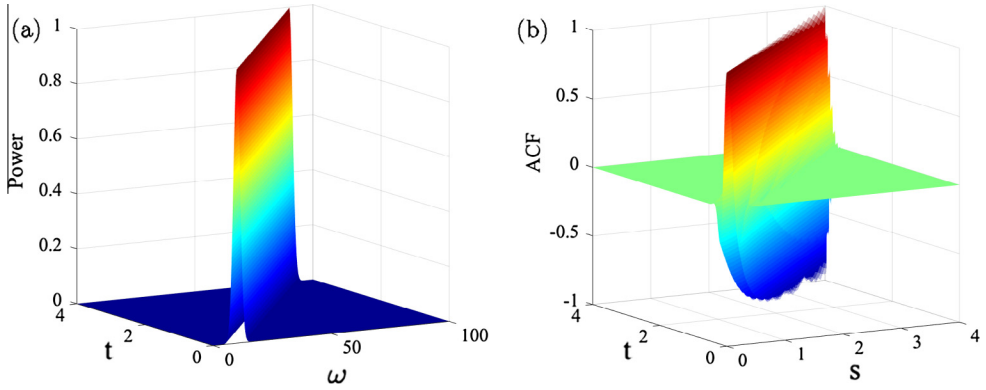

Fig. 9. Target non-Gaussian and non-stationary (a) ES and (b) ACF.

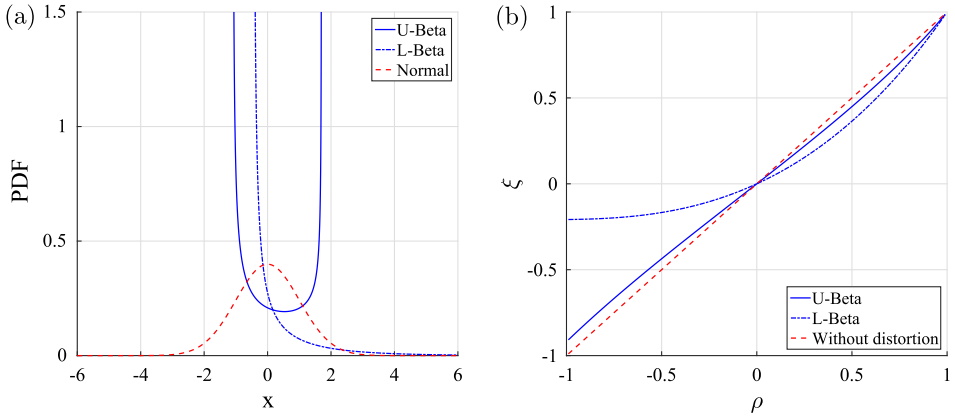

Fig. 10. (a) Two different beta PDFs and (b) the corresponding correlation distortions.

Table 2
Comparison of relative differences between the original SRM-ITAM and the proposed KL-ITAM.

Time	Relative difference, ϵ (%)			
	U-beta distribution		L-beta distribution	
	SRM-ITAM	KL-ITAM	SRM-ITAM	KL-ITAM
$t = 0$	12.798	2.4433	57.627	12.655
$t = 1$	9.3529	5.8626	69.647	52.139
$t = 2$	7.9026	6.3818	68.608	51.672

the proposed KL-ITAM converges to more accurate results than the original SRM-ITAM for strongly non-Gaussian and non-stationary processes.

8. Effect of the finding nearest PSD matrix of underlying ACF

In the iterative process to identify the underlying Gaussian ACF, the proposed method requires the additional step of identifying the nearest PSD ACF at each iteration (Section 5.4). This step

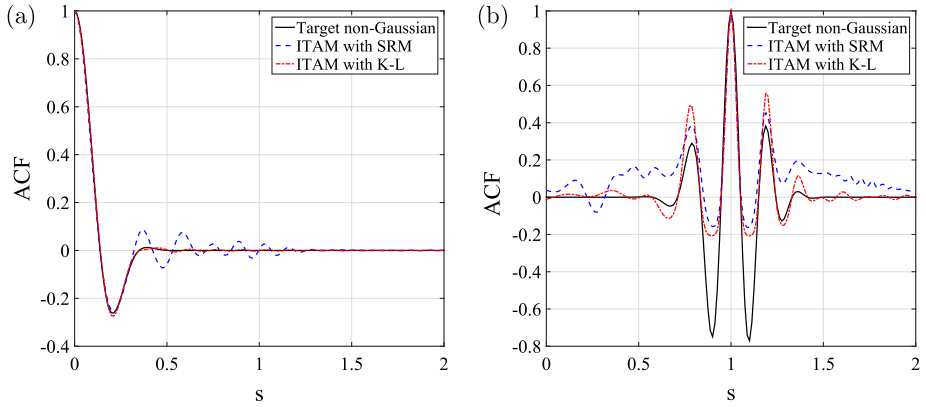

Fig. 11. Comparison of computed non-Gaussian ACFs using KL-ITAM and SRM-ITAM with (a) U-beta distribution at time $t = 0$ and (b) L-beta distribution at time $t = 1$.

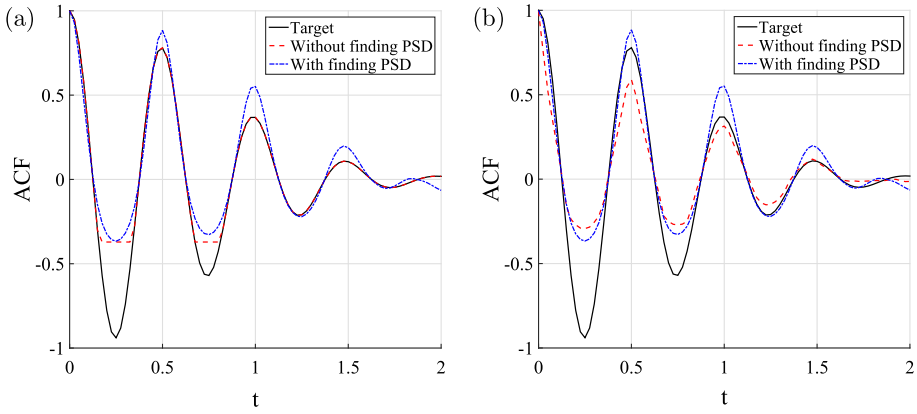

Fig. 12. (a) Computed normalized non-Gaussian ACFs after iterations with and without finding the nearest PSD ACF. (b) Estimated normalized non-Gaussian ACFs from sample functions produced using the ACFs in (a) with the K–L expansion.

ensures that the underlying Gaussian ACF remains valid and retains translation process compatibility. Since the proposed method utilizes the K–L expansion, one may be inclined to upgrade the ACF without this step and simulate the process using only the positive eigenvalues (an ACF that is not PSD will possess negative eigenvalues). However, such an approach will produce realizations that do not match well the target ACF. Fig. 12a shows the computed normalized non-Gaussian ACFs after iterations with and without finding the nearest PSD ACF. Both methods seem to converge well to the target. In fact, the non-PSD solution appears to match better the target ACF. However, Fig. 12b shows estimates of both normalized non-Gaussian ACFs, along with the target, computed from sample functions generated using the K–L expansion. Clearly, ignoring the negative eigenvalues produced by not finding the nearest PSD ACF during the iteration has a significant effect on the sample properties. The samples do not possess the ACF determined from iterations and, furthermore, possess an ACF that is less accurate than those produce using a PSD ACF. Also, not shown by the ACFs in Fig. 12 is the fact that ignoring negative eigenvalues in the simulation yields realizations with incorrect variance ($\sigma^2_{\text{without PSD}} \approx 3.3322$ from 100,000 samples compared to $\sigma^2_{\text{with PSD}} \approx 1.0062$).

Fig. 12 clearly demonstrate that finding the nearest PSD ACF is essential. But, is it necessary at every iteration or can we apply this step once at the end of iterations? Table 3 compares the accuracy of these two procedures. It is seen that finding the nearest PSD during iterations is uniformly superior for all covariances (C_1–C_8), but, with only marginal improvement in accuracy. Note that both procedures are valid schemes as they produce PSD ACFs at the end of iterations (hence no negative eigenvalues in the K–L expansion) and will therefore posses sample properties consistent with the computed ACF. However, given the low cost of finding the nearest PSD and its demonstrated improvement, it is recommended to find the nearest PSD at every iteration.

Table 3
Comparison of relative differences between the target and computed ACFs by finding the nearest PSD ACF at each iteration and finding it once at the end of iterations for a shifted lognormal distribution.

Target	Relative difference, ϵ (%)	
	Finding PSD at each iteration	Finding PSD once
Stationary		
C_1	0.0146	0.0146
C_2	0.2277	0.2388
C_3	35.393	36.596
C_4	39.925	40.028
Non-stationary		
C_5	0.0159	0.0159
C_6	0.0142	0.0142
C_7	34.450	35.217
C_8	22.685	23.380

9. Conclusions

A novel methodology has been presented for simulation of strongly non-Gaussian and non-stationary stochastic process. The presented method is based on the ITAM developed by Shields et al. [13–15] and is demonstrated to improve the accuracy of the ITAM for non-stationary processes. Both weakly and strongly non-Gaussian distributions are considered and various shapes of target ACF are utilized as numerical examples. The results demonstrate the effectiveness of the proposed algorithm for both stationary and non-stationary processes with varying degrees of translation process incompatibility. It has a series of advantages when compared with the existing simulation methods: (1) estimation of ES is not required which improves the accuracy compared with the previous ITAM procedure; (2) the convergence rate is very high; (3) the method utilizes translation process theory so that the process possesses the non-Gaussian marginal distribution exactly, and; (4) the simplicity of the ACF upgrading makes implementation straightforward.

Appendix A. Newton-CG methodology for the nearest positive semidefinite matrix

Qi and Sun [23] dualized the linear constraints in the nearest correlation matrix problem in Eq. (14) to yield the unconstrained convex optimization problem stated as:

$$\min_{y\in\mathbb{R}^n} \theta(y) := \frac{1}{2}\|(A+\text{diag}(y))_+\|_F^2 - e^T y \tag{A.1}$$

where $\text{diag}(y)$ represents the diagonal matrix with vector $y \in \mathbb{R}^n$ as its diagonal elements (this is differentiated from $\text{Diag}(\cdot)$ in Section 5.4 that extracts a vector from a matrix). The projection $(\cdot)_+$ maps symmetric matrix $B \in \mathbb{R}^{n\times n}$ with spectral decomposition $B = Q\Lambda Q^T$ where $Q^TQ = I$ and $\Lambda = \text{diag}(\lambda_i)$ onto the space of positive semidefinite matrices. The nearest positive semidefinite matrix to B in the Frobenius norm is $B_+ = Q\text{diag}(\max(\lambda_i, 0))Q^T$.

The following algorithm calculates the nearest positive semidefinite matrix $\hat{A}$ to A in the Frobenius norm with given

convergence tolerate *tol* such that $\|\nabla\theta(y_k)\|_2 \leqslant tol$ at the end of iterations. The methodology is quadratically convergent.

1. Initialize $y_0 \in \mathbb{R}^n,\ \eta \in (0,1),\ \rho,\sigma \in (0,1/2]$, and $k=0$.
2. Calculate gradient $\nabla\theta(y_k) = \mathrm{Diag}((A+\mathrm{diag}(y))_+) - e$. If $\|\nabla\theta(y_k)\|_2 \leqslant tol$, the nearest positive semidefinite matrix is $\hat{A} = (A+\mathrm{diag}(y_k))_+$ and stop.
3. Calculate the spectral decomposition $A+\mathrm{diag}(y_k) = Q\Lambda Q^T$ and generate the matrix W_{y_k} as:

$$W_{y_k} = \begin{bmatrix} E_{\alpha\alpha} & E_{\alpha\beta}\mathcal{T} \\ E_{\beta\alpha}\ 0\ 0 & \\ \mathcal{T}\ \ 0\ 0 & \end{bmatrix}, \mathcal{T} = \left(\frac{\lambda_i(y_k)}{\lambda_i(y_k)-\lambda_j(y_k)}\right)_{i\in\alpha, j\in\gamma}, \tag{A.2}$$

where $\lambda(y)$ are in descending order, the sets α,β, and γ are defined as $\alpha = \{i : \lambda_i(y_k) > 0\},\ \beta = \{i : \lambda_i(y_k) = 0\},\ \gamma = \{i : \lambda_i(y_k) < 0\}$, and $E_{\alpha\beta}$ denotes the matrix of ones of dimension $|\alpha| \times |\beta|$.
4. Determine the direction d_k by applying an iterative method to implicitly compute the generalized Jacobian $V \in \partial g(y)$:

$$V_k d_k = \mathrm{Diag}(P_{y_k}(W_{y_k} \circ (P_{y_k}^T D_k P_{y_k}))P_{y_k}^T) = -\nabla\theta(y_k) \tag{A.3}$$

where $d_k \in \mathbb{R}^n,\ D_k = \mathrm{diag}(d_k),\ P_{y_k}$ is an orthogonal matrix whose columns are the eigenvectors of $A+\mathrm{diag}(y_k)$, and the operator $\circ$ is the Hadamard product $(X \circ Y = (x_{ij}y_{ij}))$. The iterations are terminated when the following conditions are satisfied:

$$\|\nabla\theta(y_k) + V_k d_k\|_2 \leqslant \eta_k \|\nabla\theta(y_k)\|_2 \tag{A.4}$$

$$-\frac{\nabla\theta(y_k)^T}{\|d_k\|_2} \cdot \frac{d_k}{\|d_k\|_2} \geqslant \eta_k \tag{A.5}$$

where $\eta_k = \min\{\eta, \|\nabla\theta(y_k)\|_2\}$. If either one of these conditions is not satisfied, generate a new direction as

$$d_k = -B_k^{-1}\nabla\theta(y_k) \tag{A.6}$$

where B_k is any symmetric positive definite matrix with uniformly bounded $\{\|B_k\|_2\}$ and $\{\|B_k^{-1}\|_2\}$.
5. Find an appropriate step length a_k by utilizing Armijo backtracking to calculate the smallest non-negative integer m_k satisfying the following condition:

$$\theta(y_k + \rho^{m_k} d_k) \leqslant \theta(y_k) + \sigma\rho^{m_k}\nabla\theta(y_k)^T d_k \tag{A.7}$$

6. Set $\alpha_k = \rho^{m_k},\ y_{k+1} = y_k + \alpha_k d_k,\ k = k+1$, and return to step 2.

Appendix B. Supplementary data

Supplementary data associated with this article can be found, in the online version, at http://dx.doi.org/10.1016/j.compstruc.2015.08.010. These data include MOL files and InChiKeys of the most important compounds described in this article.

References

[1] Ghanem RG, Spanos PD. Stochastic finite elements: a spectral approach. Courier Corporation; 2003.
[2] Huang S, Quek S, Phoon K. Convergence study of the truncated Karhunen–Loève expansion for simulation of stochastic processes. Int J Numer Methods Eng 2001;52(9):1029–43.
[3] Phoon K, Huang S, Quek S. Simulation of second-order processes using Karhunen–Loève expansion. Comput Struct 2002;80(12):1049–60.
[4] Phoon K, Huang H, Quek S. Simulation of strongly non-Gaussian processes using Karhunen–Loève expansion. Probab Eng Mech 2005;20(2):188–98.
[5] Sakamoto S, Ghanem R. Simulation of multi-dimensional non-Gaussian non-stationary random fields. Probab Eng Mech 2002;17(2):167–76.
[6] Sakamoto S, Ghanem R. Polynomial chaos decomposition for the simulation of non-Gaussian nonstationary stochastic processes. J Eng Mech 2002;128(2):190–201.
[7] Shinozuka M, Jan C-M. Digital simulation of random processes and its applications. J Sound Vib 1972;25(1):111–28.
[8] Shinozuka M, Deodatis G. Simulation of stochastic processes by spectral representation. Appl Mech Rev 1991;44(4):191–204.
[9] Grigoriu M, Harper E. Applied non-Gaussian processes: examples, theory, simulation, linear random vibration, and MATLAB solutions. NJ: PTR Prentice Hall Upper Saddle River; 1995.
[10] Yamazaki F, Shinozuka M. Digital generation of non-Gaussian stochastic fields. J Eng Mech 1988;114(7):1183–97.
[11] Deodatis G, Micaletti RC. Simulation of highly skewed non-Gaussian stochastic processes. J Eng Mech 2001;127(12):1284–95.
[12] Bocchini P, Deodatis G. Critical review and latest developments of a class of simulation algorithms for strongly non-Gaussian random fields. Probab Eng Mech 2008;23(4):393–407.
[13] Shields M, Deodatis G, Bocchini P. A simple and efficient methodology to approximate a general non-Gaussian stationary stochastic process by a translation process. Probab Eng Mech 2011;26(4):511–9.
[14] Shields M, Deodatis G. A simple and efficient methodology to approximate a general non-Gaussian stationary stochastic vector process by a translation process with applications in wind velocity simulation. Probab Eng Mech 2013;31:19–29.
[15] Shields M, Deodatis G. Estimation of evolutionary spectra for simulation of non-stationary and non-Gaussian stochastic processes. Comput Struct 2013;126:149–63.
[16] Priestley MB. Evolutionary spectra and non-stationary processes. J Roy Stat Soc. Ser B (Methodol) 1965:204–37.
[17] Benowitz B, Shields M, Deodatis G. Determining evolutionary spectra from non-stationary autocorrelation functions. Probab Eng Mech 2015.
[18] Betz W, Papaioannou I, Straub D. Numerical methods for the discretization of random fields by means of the Karhunen–Loève expansion. Comput Methods Appl Mech Eng 2014;271:109–29.
[19] Grigoriu M. Probabilistic models for stochastic elliptic partial differential equations. J Comput Phys 2010;229(22):8406–29.
[20] Ferrante F, Arwade S, Graham-Brady L. A translation model for non-stationary, non-Gaussian random processes. Probab Eng Mech 2005;20(3):215–28.
[21] Shampine L. Matlab program for quadrature in 2d. Appl Math Comput 2008;202(1):266–74.
[22] Higham NJ. Computing the nearest correlation matrix—a problem from finance. IMA J Numer Anal 2002;22(3):329–43.
[23] Qi H, Sun D. A quadratically convergent newton method for computing the nearest correlation matrix. SIAM J Matrix Anal Appl 2006;28(2):360–85.
[24] Borsdorf R, Higham NJ. A preconditioned newton algorithm for the nearest correlation matrix. IMA J Numer Anal 2010;30(1):94–107.